remote sensing

MDPI

Article

High-Resolution Monitoring of Live Fuel Moisture Content Across Australia

Marta Yebra [1,2,*], Gianluca Scortechini [1], Nicolas Younes [1] and Albert I. J. M. van Dijk [1]

[1] The Fenner School of Environment & Society, College of Systems & Society, The Australian National University, Linnaeus Way, Acton, ACT 2601, Australia
[2] School of Engineering, College of Systems & Society, The Australian National University, Canberra, ACT 2601, Australia
* Correspondence: marta.yebra@anu.edu.au

Highlights

What are the main findings?

- This study demonstrates the feasibility of producing a nationally consistent, high resolution (20 m), and frequently updated operational Live Fuel Moisture Content (LFMC) product for Australia using Sentinel-2.
- Model performance varies across vegetation types and is primarily influenced by site homogeneity and sampling representativeness; temporal mismatch (±3–10 days) has limited effect.

What are the implications of the main findings?

- Absolute LFMC estimates are most reliable in homogeneous sites, whereas in heterogeneous landscapes the product is better suited for monitoring relative spatial and temporal variations in LFMC.
- The product can support operational decision-making, (e.g., hazard reduction, cultural burning, fire breaks, modelling ignition and complement potential and existing land management practices).

Abstract

Live Fuel Moisture Content (LFMC) is a key determinant of vegetation flammability and fire behaviour, yet LFMC products have traditionally relied on coarse-resolution sensors such as the Moderate Resolution Imaging Spectroradiometer (MODIS, 500 m), limiting their utility for fine-scale fire management. This study introduces the first continental-scale operational LFMC product for Australia derived from Sentinel-2 imagery at 20 m resolution. We developed a Random Forest regression model trained on approximately 680,000 paired Sentinel-2 reflectance and MODIS-LFMC samples (2015–2022) to emulate outputs from the Australian Flammability Monitoring System (AFMS), a MODIS-based pre-operational LFMC product. Model evaluation against AFMS showed strong agreement for grasslands (R^2 = 0.83, RMSE = 32.45%) and moderate performance for forests (R^2 = 0.43, RMSE = 20.84%) and shrublands (R^2 = 0.21, RMSE = 10.28%). Validation using 2279 in situ LFMC measurements from Globe-LFMC 2.0 indicated improved accuracy at homogeneous sites (NDVI CV $\leq$ 20th percentile: R^2 = 0.42, RMSE = 31.39%). Additionally, when validating with a dedicated field campaign specifically designed for Sentinel-2 LFMC assessment, the model achieved its highest accuracy (R^2 = 0.53, RMSE = 32.14%), highlighting the importance of tailored ground protocols for satellite product validation. Predicted LFMC also reproduced observed seasonal dynamics at sites with frequent field monitoring. Despite variability across vegetation types, the Sentinel-2 LFMC product

Check for updates

Academic Editors: Kevin Tansey and Jungho Im

Received: 5 January 2026
Revised: 23 March 2026
Accepted: 25 March 2026
Published: 31 March 2026

Copyright: © 2026 by the authors. Licensee MDPI, Basel, Switzerland. This article is an open access article distributed under the terms and conditions of the Creative Commons Attribution (CC BY) license.

effectively captured spatial patterns and seasonal dynamics, providing a step change in monitoring vegetation moisture at landscape scales. This high-resolution dataset offers actionable intelligence for prescribed burning, fuel treatment planning, and fire behaviour modelling in fire-prone environments.

Keywords: fire management; fire behaviour; vegetation dryness; vegetation flammability; seasonal dynamics

1. Introduction

Live Fuel Moisture Content (LFMC) is a critical determinant of vegetation flammability and fire behaviour, influencing ignition potential, fire spread, and severity [1–3]. Accurate LFMC estimation is essential for operational fire management planning, including prescribed burning, treatment prioritisation, and containment planning, as well as wildfire risk modelling [4,5]. Remote sensing has enabled large-scale LFMC monitoring, but existing approaches face limitations in spatial resolution and computational efficiency [6].

Optical remote sensing has historically been the primary domain for LFMC estimation, exploiting the sensitivity of vegetation water content to reflectance variations in the shortwave infrared (SWIR) and near-infrared (NIR) regions [3]. Retrieval strategies generally rely on radiative transfer model (RTM) inversions and empirical techniques, including machine learning and statistical models [5,7–9]. RTM-based methods provide strong theoretical foundations but are computationally demanding, especially at high spatial resolutions. Empirical models are computationally efficient but depend on geographically biassed ground samples, limiting global applicability.

The Moderate Resolution Imaging Spectroradiometer (MODIS) has been the primary sensor for LFMC modelling due to its daily observations and long-term data record [3]. In Australia, the Australian Flammability Monitoring System (AFMS) is the only MODIS-based LFMC product operating in a pre-operational capacity [5]. AFMS estimates LFMC using vegetation-type-specific look-up tables (LUTs) for forests, shrub-lands, and grasslands. For each pixel, the 40 most spectrally similar entries are selected from the LUT, and the median LFMC of those entries is used as the final estimate. The number of selected spectra was determined through sensitivity analysis to maximise R^2 and minimise RMSE against field observations. [5]. While effective, this approach is computationally intensive and constrained by the 500 m spatial resolution of MODIS data, which limits its suitability for fine-scale fire management. Additionally, in heterogeneous landscapes, a single MODIS pixel may encompass multiple vegetation types and microclimates, reducing retrieval accuracy.

Alternative sensors have been explored, such as the Advanced Himawari Imager (AHI), which provides sub-daily observations useful for short-term moisture dynamics [10]. However, this increased temporal frequency comes at the cost of spatial resolution (2 km), which is even coarser than MODIS and restricts its applicability for detailed landscape-scale assessments. Together, MODIS- and AHI-based approaches illustrate the fundamental trade-off between temporal frequency and spatial detail for operational LFMC monitoring. While both remain valuable for continental-scale fire season outlooks and strategic planning, their coarse spatial resolution limits their utility for fine-scale fuel management and tactical fire planning.

The launch of Sentinel-2 in 2015 under the Copernicus Programme introduced multispectral imagery at 10–20 m resolution and red-edge bands, which are particularly sensitive

to vegetation structure and pigment dynamics [11], thereby offering a significant opportunity to improve LFMC mapping at fine scales.

Recent studies have applied both RTM inversion frameworks and empirical approaches to Sentinel-2 reflectance for site-level or regional LFMC retrievals [12–14], in some cases incorporating meteorological variables [15], or Sentinel-1 radar backscatter [16]. While investigations demonstrate strong potential for high-resolution LFMC estimation, their implementation has typically focused on specific species or homogeneous vegetation types and remains geographically constrained. Empirical approaches offer a computationally efficient solution and are relatively straightforward to deploy over large spatial domains. However, their transferability across ecosystems and climatic gradients is often limited, as model performance depends strongly on the representativeness of the training data. Although global datasets such as Globe-LFMC 2.0 [17] substantially improve data availability, the spatial and ecological distribution of LFMC measurements remains uneven worldwide, which can constrain model generalisation in underrepresented vegetation types or climatic regions without additional recalibration.

In contrast, physically based inversion methods grounded in RTM theory are less reliant on local calibration and may offer stronger theoretical transferability. Nevertheless, applying full RTM inversion at Sentinel-2 spatial resolution remains computationally demanding, particularly when extended to continental-scale domains.

Two conceptually distinct approaches can be followed when generating satellite-based LFMC products: (i) direct physical or semi-physical estimation of LFMC from reflectance using radiative transfer inversion or empirical relationships calibrated against field data, and (ii) operational product emulation, in which a higher-resolution sensor is trained to reproduce the behaviour of an existing, validated LFMC monitoring system. The first approach aims to retrieve LFMC as a biophysical variable directly from spectral signals, whereas the second prioritises consistency, scalability, and operational continuity with an established framework. These approaches differ not only in methodology but also in their intended application and evaluation criteria.

Building on this operational perspective, we adopted the emulator strategy to develop the first continental-scale LFMC product for Australia, derived from Sentinel-2 imagery at 20 m resolution. Specifically, Sentinel-2 reflectance is used to emulate the behaviour of the pre-operational Australian Flammability Monitoring System (AFMS). A Random Forest regression model was trained on approximately 680,000 paired Sentinel-2 reflectance and MODIS-LFMC samples (2015–2022) to reproduce AFMS-derived LFMC patterns at higher spatial resolution. Rather than directly estimating LFMC from first principles, this approach preserves the operational logic and long-term consistency of AFMS while enhancing spatial detail and computational efficiency.

Model performance was assessed against AFMS and 2279 in situ LFMC measurements from Globe-LFMC 2.0. Further, a dedicated Sentinel-2 evaluation campaign, comprising a subset of Globe-LFMC 2.0 samples collected specifically for Sentinel-2-based LFMC estimations, was used to assess the model performance under controlled sampling conditions. Finally, we assessed the model's ability to reproduce temporal LFMC dynamics by visually comparing predicted and observed LFMC time series at Globe-LFMC 2.0 sites with long-term repeated measurements.

The Sentinel-2 LFMC product establishes the first operational framework for high-resolution LFMC mapping across Australia, bridging the gap between coarse-resolution MODIS products and the fine-scale requirements of fire management. The product captures spatial patterns and seasonal LFMC dynamics, providing relevant actionable insights for prescribed burning, fuel treatment planning, and fire behaviour modelling in fire-prone

landscapes. It is designed for operational deployment and is currently distributed through Digital Earth Australia as regularly updated 5-day mosaics [18].

2. Methods

A high-resolution (20 m) Live Fuel Moisture Content (LFMC) product for Australia was developed using Sentinel-2 surface reflectance. The workflow comprised three main steps: (i) data acquisition and preprocessing, (ii) model development and hyperparameter optimisation, and (iii) validation against both an operational MODIS-based product (AFMS) and in situ measurements (Figure 1).

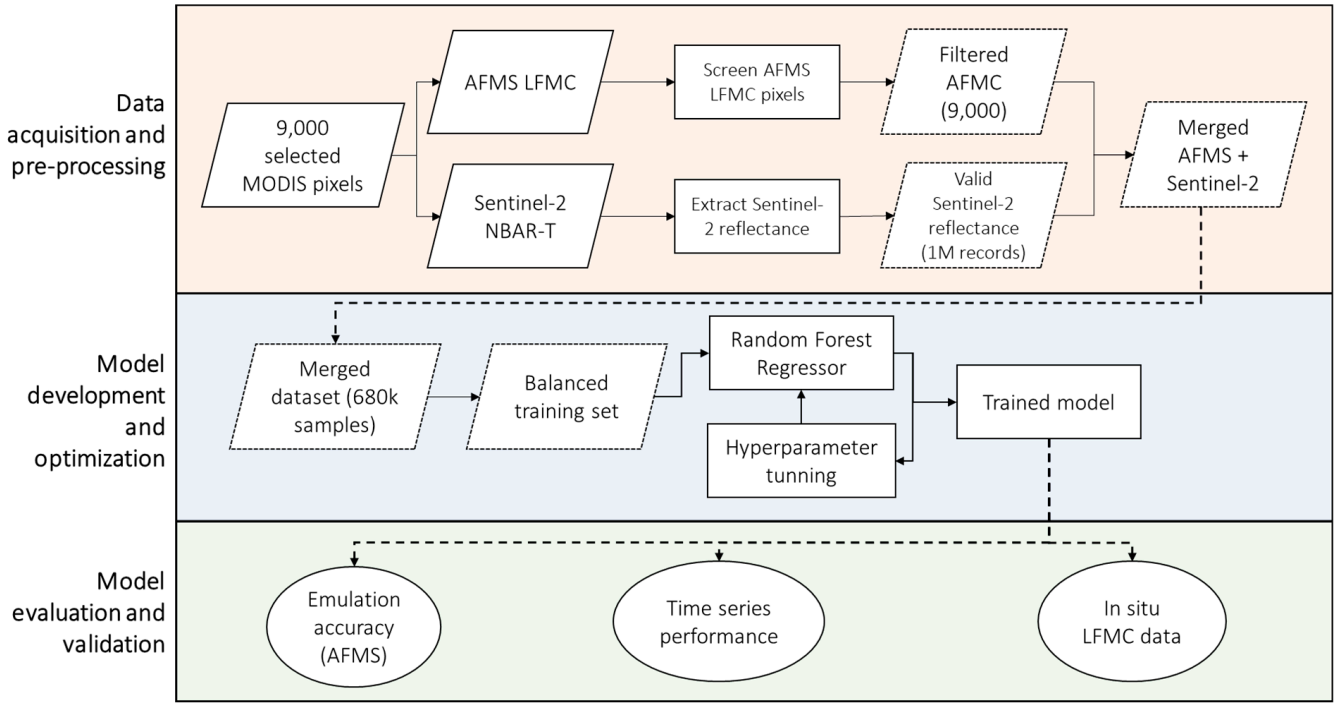


Figure 1. Workflow illustrating the development and validation of the Sentinel-2 LFMC product. The process includes three main steps: (i) data acquisition and preprocessing of MODIS-derived LFMC and Sentinel-2 reflectance data, (ii) model development and hyperparameter optimisation using a Random Forest regressor, and (iii) validation against the Australian Flammability Monitoring System (AFMS) and in situ LFMC measurements from Globe-LFMC 2.0 and a dedicated field campaign.

All data extraction, model development, and validation were implemented in Python (v3.x), leveraging the scikit-learn library (v1.1.2) [19] for machine learning. To ensure reproducibility, all scripts and implementation details are openly available at https://github.com/BRCoE/sentinel2_FMC_emulator_v2 (accessed on 20 March 2025).

2.1. Data

2.1.1. AFMS LFMC Data

LFMC estimates from the Australian Flammability Monitoring System (AFMS) served as the response variable for model training. AFMS uses MODIS MCD43A4 reflectance [20] and vegetation-type-specific look-up tables to estimate LFMC for forests, shrublands, and grasslands [5]. The product has a spatial resolution of 500 m and a 4-day temporal frequency, with a time series that starts at the beginning of each year. Data spanning 2015–2022 were extracted from the National Computational Infrastructure THREDDS catalogue (https://thredds.nci.org.au/thredds/catalog/ub8/au/FMC/catalog.html, accessed on 20 September 2023) at the time of writing). The analysis period begins in 2015, coinciding

with the first availability of Sentinel-2 data, and extends to 2022, the year of the most recent MODIS land cover product available at the time of this study.

2.1.2. Sentinel-2 Reflectance Data

Predictor variables were derived from Sentinel-2 surface reflectance (NBART—Nadir corrected Bidirectional reflectance distribution function Adjusted Reflectance Terrain corrected) product Collection 3 available through Digital Earth Australia (DEA) analysis-ready data cube [21,22]. NBART is a correction applied by the DEA to compensate for terrain illumination effects and shadowing [21]. This pre-processing ensures consistency in the reflectance values used as model inputs. Ten spectral bands (Blue, Green, Red, three Red-edge, NIR, NIR narrow, SWIR1, SWIR2) were used, along with the Normalised Difference Vegetation Index (NDVI) [23] and the Normalised Difference Infrared Index (NDII) [24]. Given that Sentinel-2 bands have different spatial resolutions (i.e., 10 m for visible and near infrared bands, and 20 m for red edge and shortwave infrared bands), all data were loaded at 10 m using the 'nearest' resampling method in DEA [25] for feature calculations, with the final product output released at 20 m resolution. Cloud, shadow, snow, and water pixels were masked using DEA quality flags.

2.1.3. Globe LFMC2.0

Independent validation used LFMC measurements from Globe-LFMC 2.0 [17], a harmonised global database of field-measured LFMC. Samples collected in Australia between July 2015 and December 2022 were extracted, quality-filtered, and averaged by site and date, resulting in 197 independent LFMC values suitable for validation. From this broader pool, we further isolated a subset of measurements that had been collected specifically to validate Sentinel-2-derived LFMC estimates during targeted field campaigns designed for satellite product assessment. These campaign-focused samples were treated separately and used to evaluate the model's performance under conditions that tightly controlled the temporal alignment between field measurements and satellite overpasses. A detailed description of these targeted validation data, including sampling design, measurement protocol, and final sample size, is provided in [26], from which the corresponding subset was extracted.

2.2. Sampling Design, Data Extraction, and Merging

2.2.1. Filtering and Selection of AFMS LFMC Training Pixels

MODIS-Based AFMS LFMC training pixels associated with each vegetation class (forest, shrubland, and grassland) were identified for the 2015–2022 period. To ensure adequate temporal density for machine learning, only pixels with $\geq$90% valid LFMC values were retained. This threshold was applied to reduce the influence of temporal gaps on model performance and to ensure consistent representation of seasonal LFMC dynamics across years.

To minimise mixed-pixel and edge effects at the MODIS 500 m resolution, pixels were included only when all eight surrounding pixels in a 3 $\times$ 3 window belonged to the same vegetation class. This neighbourhood criterion ensured that reflectance and LFMC signals corresponded to homogeneous vegetation, thereby reducing uncertainty introduced by sub-pixel land-cover mixing.

Following this filtering, 3000 geographically dispersed pixels per vegetation type (9000 total) were selected (Figure 2). This sample size was chosen to provide (i) balanced representation of the three vegetation classes, (ii) coverage across Australia's environmental gradients, and (iii) computational tractability for model training given the multi-million-sample dataset. Pixels located outside Australia due to MODIS tile boundaries were excluded.

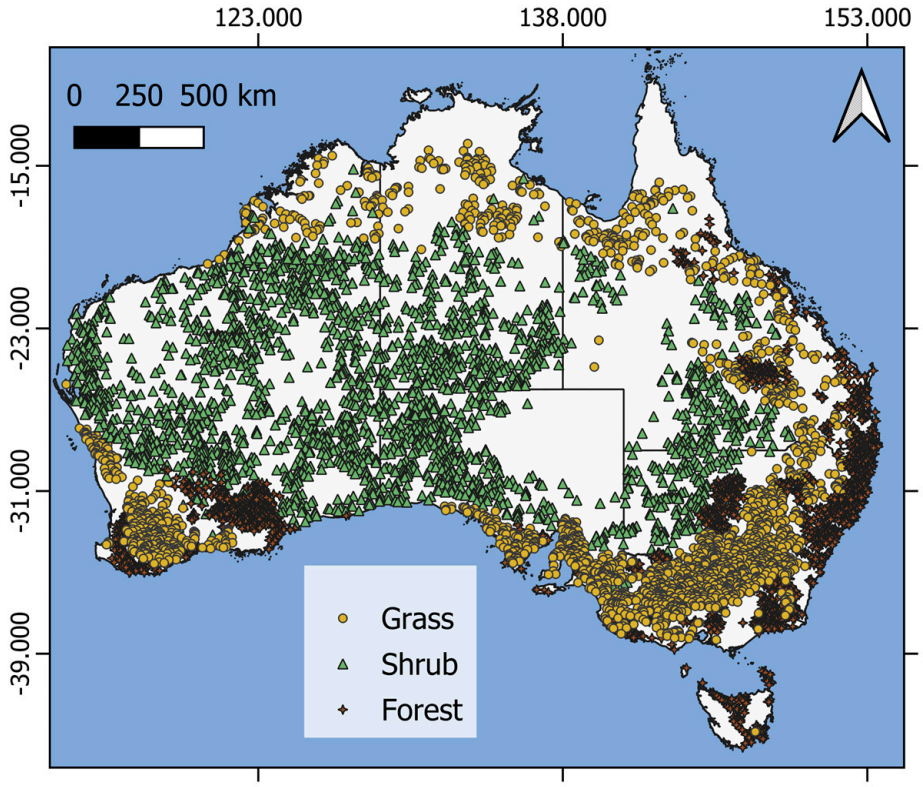


Figure 2. Geographical distribution of selected sites used for AFMS LFMC extraction and Sentinel-2 model training.

For each selected pixel, the complete time series of valid AFMS LFMC values was extracted, resulting in approximately 6.5 million LFMC measurements available for modelling.

2.2.2. Sentinel-2 Surface Reflectance Extraction

Sentinel-2 surface reflectance NBART from Digital Earth Australia was extracted for each AFMS LFMC pixel to provide the predictor variables required for model training. To ensure that the Sentinel-2 observations corresponded spatially to the AFMS LFMC estimates, a 500 m × 500 m extraction window was defined around the central coordinate of each AFMS (MODIS) pixel. That central coordinate was used to select all Sentinel-2 pixels located within each 500 m × 500 m window; the mean values for each band were calculated for the selected pixels, thus ensuring that the higher-resolution Sentinel-2 reflectance values were matched to the footprint of the coarser AFMS pixel. This approach also reduced the influence of geolocation mismatch between sensors and mitigated the effects of sub-pixel heterogeneity in the Sentinel-2 data.

For each Sentinel-2 scene, all pixels falling within the extraction window were retrieved and subjected to quality filtering. Pixels flagged as cloud, cloud shadow, snow, or water were removed, and the quality masks were conservatively dilated by approximately 200 m to minimise contamination from thin cloud edges or residual shadow artefacts. Scenes in which fewer than 75% of the pixels in the extraction window remained valid after masking were discarded to ensure that the resulting spatial averages were representative of the MODIS footprint. For all retained scenes, mean reflectance values were computed for each spectral band and vegetation index. Using this procedure, more than one million valid Sentinel-2 observations were obtained across all sites.

2.2.3. Merging Sentinel-2 and AFMS LFMC

Sentinel-2 and AFMS LFMC datasets were merged using exact date matching. Records were retained only when both datasets contained an observation on the same date, avoiding temporal interpolation. The merged dataset comprised approximately 680,000 paired samples, each consisting of a Sentinel-2 reflectance vector and an AFMS LFMC value.

Although equal numbers of AFMS sites were selected per vegetation class, the final merged dataset was imbalanced due to spatial variation in cloud cover affecting Sentinel-2 availability. Approximately 175,000 samples corresponded to forests, 285,000 to shrublands, and 220,000 to grasslands (Figure S2).

2.3. Sentinel-2 LFMC Model Development

2.3.1. Data Partitioning for Training and Testing

The merged AFMS–Sentinel 2 dataset was divided into training and test subsets, ensuring the datasets accurately reflected the overall LFMC values distribution and were representative of the three vegetation types (grasslands, shrublands, forest). Because the number of available samples differed substantially across vegetation types, shrubland and grassland records were randomly sub-sampled to match the number of forest samples. This yielded a balanced dataset for model development, while the non-selected records were retained to contribute to the testing set (Figure S2).

A stratified sampling approach was then applied to the balanced dataset to ensure the distribution and frequency of the balanced dataset were reflected in the subsequent training and testing subsets (Figure S2). We selected 80% of the samples for training, while maintaining the original LFMC value distribution within each vegetation class. The remaining 20% of the balanced dataset was subsequently combined with the previously-excluded shrubland and grassland samples to form the final testing dataset, which was unbalanced in terms of the number of samples for each vegetation type (Figures 2 and S2). As a result, the training set represented approximately 60% of all available samples, while the remaining 40% formed the test set (Figures S2 and 1). This procedure ensured that (i) model training was not biassed toward the most abundant vegetation classes, and (ii) model evaluation used an LFMC distribution closer to real-world conditions, where vegetation classes are unevenly represented.

2.3.2. Random Forest Modelling and Hyperparameter Optimisation

The RandomForestRegressor algorithm from Scikit-Learn [19] was employed to develop the LFMC prediction model. Given the large volume of training samples, traditional hyperparameter tuning approaches such as GridSearchCV or RandomizedSearchCV were deemed computationally expensive. Grid search systematically evaluates all possible combinations of predefined hyperparameters, applying cross-validation across the entire training dataset, whereas randomised search selects hyperparameter values randomly from a broad range, reducing computational cost but still requiring extensive training time.

To improve efficiency while ensuring a thorough exploration of the hyperparameter space, HalvingRandomSearchCV (successive halving search) [27] was employed. This method initially evaluates a large set of hyperparameter combinations using a subset of the training data, while progressively filtering out underperforming models and increasing the number of training samples used at each iteration. The process iteratively increases the training data size for the retained models until the final set is validated on the full dataset.

The hyperparameter ranges explored during the successive halving search are listed in Table 1.

Table 1. Hyperparameter ranges considered during the randomised successive halving search.

Hyperparameter	Explanation	Range of Possible Values
n_estimators	Number of trees	Random integer from 10 to 149
criterion	Splitting criterion	'squared_error', 'absolute_error', 'friedman_mse', 'poisson'
max_depth	Maximum depth of each tree	Random integer from 5 to 49
min_samples_split	Minimum samples required to split an internal node. A split is made only if the number of samples is in a node	Random integer from 2 to 49
min_samples_leaf	Minimum samples required in each leaf node. A split is made only if the resulting leaves will have at least this number of samples	Random integer from 1 to 29
max_features	Number of features considered at each split	Random integer from 1 to the total number of features minus one
bootstrap	Whether bootstrap sampling is used	True, False

2.3.3. Hyperparameter Tuning and Final Model Selection

HalvingRandomSearchCV was first applied to a 1% subset of the training dataset, consisting of approximately 4200 samples, to reduce computational cost. This subset was selected using the same method as the training-test split to ensure a balanced representation across vegetation classes while preserving the distribution of LFMC values.

The hyperparameter search began with 1000 randomly generated hyperparameter combinations, initially evaluated using 466 samples. Successive iterations progressively refined the search space, with the final iteration comparing 112 hyperparameter sets using 4194 samples. A 5-fold cross-validation was employed to assess model performance, with Root Mean Square Error (RMSE) as the scoring metric.

Following this initial selection of hyperparameters in the 1% subset, the most promising hyperparameter values identified through successive halving were refined using a comprehensive GridSearchCV with a 3-fold cross-validation applied to the entire training dataset (416 k samples, Figure S2), thus allowing the model to learn from all the data available. Based on the results of this second tuning stage, certain hyperparameters were fixed. The criterion was set to "squared_error," the minimum number of samples required to split an internal node was set to 11, the minimum number of samples per leaf node was set to 4, and the number of features considered for each split was fixed at 9. The model was also configured to use bootstrapping.

Conversely, the number of trees in the forest (n_estimators) and the maximum depth of each tree (max_depth) were evaluated in greater detail to determine whether smaller, computationally simpler models could achieve comparable performance. In addition to the values emerging from the successive halving search (76 trees, depth 24), several reduced configurations were tested (15 or 25 trees; maximum depth 5, 10, or 15).

Fine-tuning results revealed that several smaller models performed nearly as well as the best-performing, but more complex, model from the initial search. As a result, model size—defined by the number of trees and the maximum tree depth—was introduced as an additional criterion for final model selection. The objective was to identify a model that maintained high predictive accuracy while reducing computational cost. The final model was chosen based on the best combination of number of trees (i.e., fewer is better), RMSE (i.e., lower is better), and R^2 values (i.e., higher is better). Based on these criteria, the selected model had a maximum tree depth of 24 and 15 trees, striking a balance between computational efficiency and predictive performance.

2.4. Model Validation

Model performance was evaluated using three complementary approaches: (i) emulation accuracy, quantitative, assessing the ability of the model to reproduce AFMS-derived LFMC values, (ii) independent quantitative validation using in situ LFMC measurements from Globe-LFMC 2.0 [17], and (iii) temporal validation, qualitative assessment of the model's ability to capture temporal LFMC dynamics using Globe-LFMC 2.0 sites with long-term repeated measurements.

Across all quantitative validation approaches, model accuracy was quantified using the Root Mean Squared Error (RMSE) and the coefficient of determination (R^2), which together assess both absolute accuracy and the model's ability to capture the variability of the AFMS-derived LFMC values.

2.4.1. Emulation Accuracy (Sentinel-2 LFMC Versus AFMS LFMC)

The first evaluation quantified how well the model reproduced AFMS LFMC estimates. Predictions were compared to AFMS LFMC for (i) the full test dataset, (ii) each vegetation class (grassland, shrubland, forest) separately, and (iii) a balanced subset of approximately 100,000 test samples with equal representation across vegetation types. This ensured that the performance metrics were not dominated by the vegetation classes with the highest sample counts.

2.4.2. Independent Quantitative Validation Using In Situ LFMC Measurements

From the complete Globe-LFMC 2.0 database (>280,000 global samples), 2372 Australian measurements across 42 sites collected between October 2015 and December 2022 were retained after filtering, applying dataset quality flags. The MODIS-based land cover classification was reviewed for several samples and updated to the land cover type observed on the site. These were aggregated by site and date, resulting in 197 independent LFMC values for validation.

LFMC was predicted by applying the Random Forest model to Sentinel-2 imagery within a 40 m × 40 m buffer (i.e., 2 × 2 pixels) around each sample location, mitigating sub-pixel location uncertainty (Figure S1). Sentinel-2 acquisitions within ±3, ±5, and ±10 days of each sampling date were considered, and the nearest valid date was selected. Predicted LFMC was summarised as the median of all valid pixels within the buffer. Model performance reported in the main manuscript was assessed using the ±10-day time window, which included all available validation samples. Additional sensitivity analyses using shorter windows (±3 and ±5 days) and different homogeneity criteria were conducted to evaluate the effect of temporal mismatch between field sampling and satellite acquisition; these results are reported in Supplementary Section S2 and Table S2.

Site homogeneity was quantified using NDVI from Sentinel-2 data within the same buffer areas, and the coefficient of variance (henceforth NDVI CV) as follows:

$$\text{NDVI_CV} = \sigma/\mu \times 100; \quad (1)$$

where σ is the standard deviation, and μ is the mean of the NDVI values of all pixels within a buffer area.

The NDVI_CV provides an estimate of the representativeness of in situ plot-scale 1, for remote sensing validation [28]. A higher NDVI CV could be indicative of a heterogeneous site; thus, the ground samples collected in those locations might be less representative of the signal received by the satellite sensor. To assess the influence of heterogeneity, validation was performed for (i) all samples, (ii) vegetation classes separately (grassland, shrubland, forest), and (iii) NDVI_CV decile thresholds (10th percentile to 100%).

For the aggregation per vegetation classes, and to ensure consistency between in situ measurements and AFMS vegetation types, all ground samples were harmonised using MODIS-based International Geosphere-Biosphere Programme (IGBP) classification [29], following AFMS vegetation groupings [5] with additional filtering to ensure consistency between functional types contributing to Sentinel-2 reflectance and site-level LFMC measurements. Full details of the harmonisation workflow, including class-specific filtering rules and special cases, are provided in Supplementary Section S1.

Model performance was also evaluated using a subset of Globe-LFMC 2.0 (24 sites, 707 observations), which originates from a dedicated field campaign explicitly designed for evaluating Sentinel-2 LFMC retrievals in Australian ecosystems [26]. These samples were analysed to provide a controlled, sensor-targeted validation dataset.

2.4.3. Temporal Validation Using Long-Term LFMC Time Series

To evaluate the ability of the model to reproduce seasonal LFMC dynamics, predicted LFMC time series were visually compared with long-term repeated LFMC measurements from Globe-LFMC 2.0. These comparisons examine the model's capacity to track drying and recovery patterns, peak LFMC, and seasonal transitions. Six sites across New South Wales and Western Australia were identified having 866 observations.

3. Results

The primary aim of this work is to demonstrate the enhanced spatial detail provided by the Sentinel-2-derived LFMC product when compared to the MODIS-based AFMS product. The improvement in spatial resolution of the Sentinel-2 LFMC product is evident in Figure 3, which shows the Koi Kyenunuruff region in Western Australia (also known as Stirling Range National Park). This landscape comprises a heterogeneous mixture of shrublands, mallee-heath, and woodlands surrounded by an agricultural mosaic.

The finer spatial resolution of the Sentinel-2 LFMC product (20 m) enables the differentiation of individual land plots, roads, and sharp transitions between different vegetation types (Figure 3C). In contrast, the coarser 500 m resolution of the AFMS product (Figure 3D) results in substantial spatial aggregation, limiting the ability to resolve landscape heterogeneity.

3.1. Emulation Accuracy and Feature Importance

The Sentinel-2 LFMC emulator reproduced the AFMS-derived LFMC with high overall accuracy across balanced and the full (unbalanced) datasets. When evaluated on the balanced dataset, the model yielded an RMSE of 22.92% and R^2 = 0.83. Comparable performance was observed for the full (unbalanced) test dataset (RMSE = 21.01% and R^2 = 0.84), indicating that the balancing strategy applied during training did not compromise generalisation ability. The slightly higher accuracy for the unbalanced dataset is likely influenced by the larger proportion of grassland samples, which represent the vegetation type the model predicts most accurately (see Supplementary Materials).

Model performance varied among vegetation types (Figure 4). Grasslands showed the strongest agreement, with predictions closely following AFMS LFMC across most of the observed range (R^2 = 0.83, RMSE = 32.41%). Predictions remained well distributed around the 1:1 line, although some biases occurred mainly at the extremes, where the model slightly underestimated very high LFMC values (~300%) and overestimated very low values (<10%).

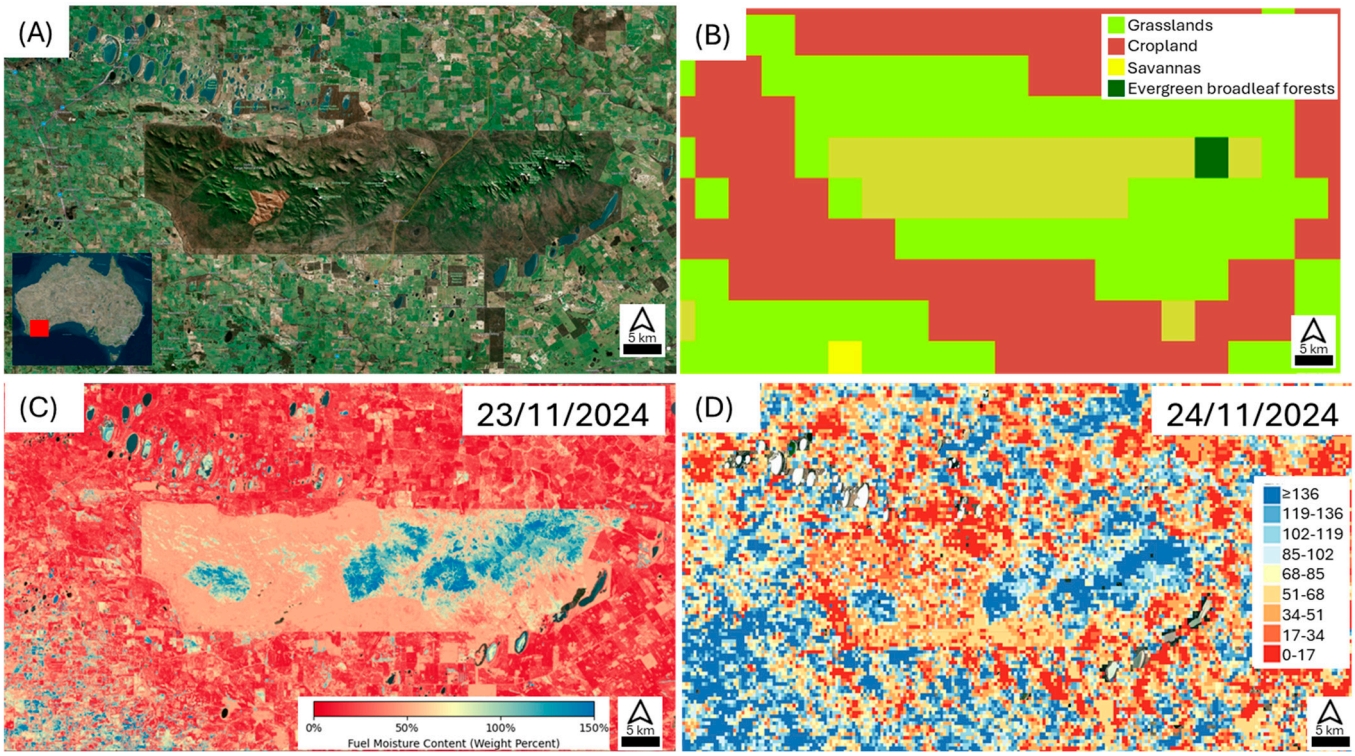


Figure 3. Side-by-side comparison of the MODIS and the Sentinel-2 LFMC products. Panel (**A**): High-resolution basemap of Koi Kyenunu-ruff (Stirling Range National Park, Western Australia) and surrounding areas. Panel (**B**): MODIS IGBP land cover classification for 2024. Panel (**C**): Sentinel-2-based LFMC estimation (23 November 2024). Panel (**D**): MODIS-based LFMC estimation from the AFMS (24 November 2024). High-resolution imagery basemap provided by Bing Maps through Digital Earth Australia for reference only and not used for analysis. Note that the Bing Maps basemap represents imagery acquired on different dates (including 1999–2003) and does not correspond temporally to the LFMC products shown.

Forests showed moderate performance (R^2 = 0.43, RMSE = 20.84%). The densest portion of the predicted–observed point cloud aligned closely with the 1:1 relationship, though a general tendency to underestimate LFMC was evident across the distribution.

Shrublands exhibited the weakest agreement (R^2 = 0.21), with systematic overestimations at AFMS values >80%. However, because shrubland LFMC in the AFMS product spans a relatively narrow range (~0–150%), which limits the magnitude of absolute errors, and explains the relatively low RMSE (10.27%) despite modest explanatory power.

To examine the geographical performance of the model, we calculated the residuals for each training data point (Figure 5) by subtracting the Sentinel-2 LFMC from the MODIS-based LFMC. In general, the residuals are normally distributed (μ = 2.7, σ = 22.1, Figure S4); the spatial distribution of the residuals (Figure 5) does not reveal systematic biases in particular regions of the continent, but it does reveal a distribution that resembles the vegetation type (Figure 5, see more in Section 4.3).

Feature importance analysis indicated that NDII was the most influential predictor in the final Random Forest model according to both Gini and permutation importance metrics (Figure S3). NDII is derived from the Sentinel-2 NIR and SWIR2 bands, and individual SWIR bands ranked lower, likely reflecting their strong correlation with the index.

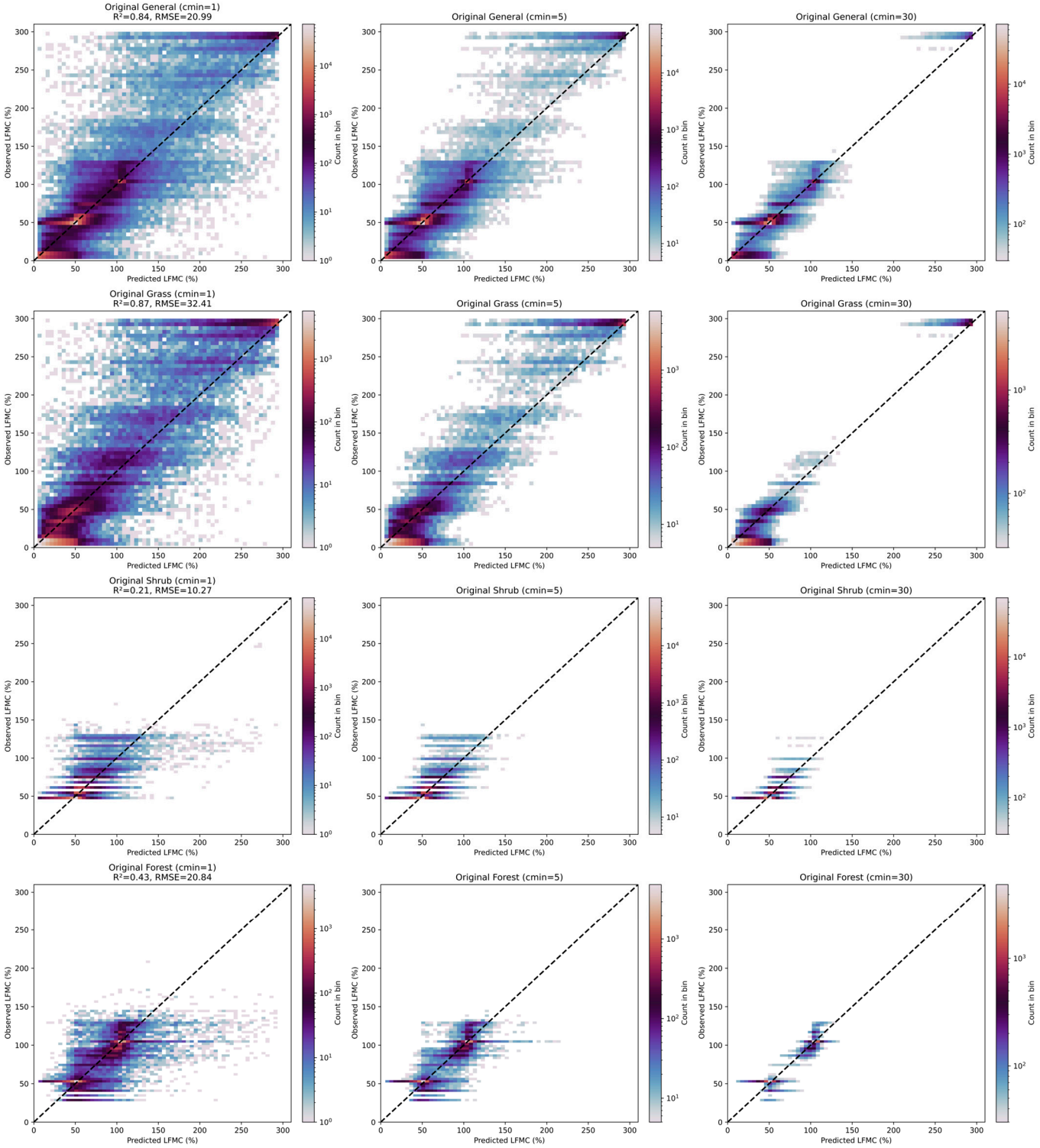


Figure 4. Predicted versus observed LFMC for the Random Forest model emulating the MODIS-based AFMS product. Density scatterplots show the relationship between Sentinel-2-derived LFMC predictions and AFMS LFMC for grasslands, shrublands, and forests in the test dataset. Colours represent point density, with 'cmin' indicating the minimum number of observations required for a bin to be displayed. The model shows strong agreement for grasslands, moderate agreement for forests, and weaker performance for shrublands, which display a narrower AFMS LFMC range and a tendency toward overestimation. Dashed line represents the 1:1 relationship.

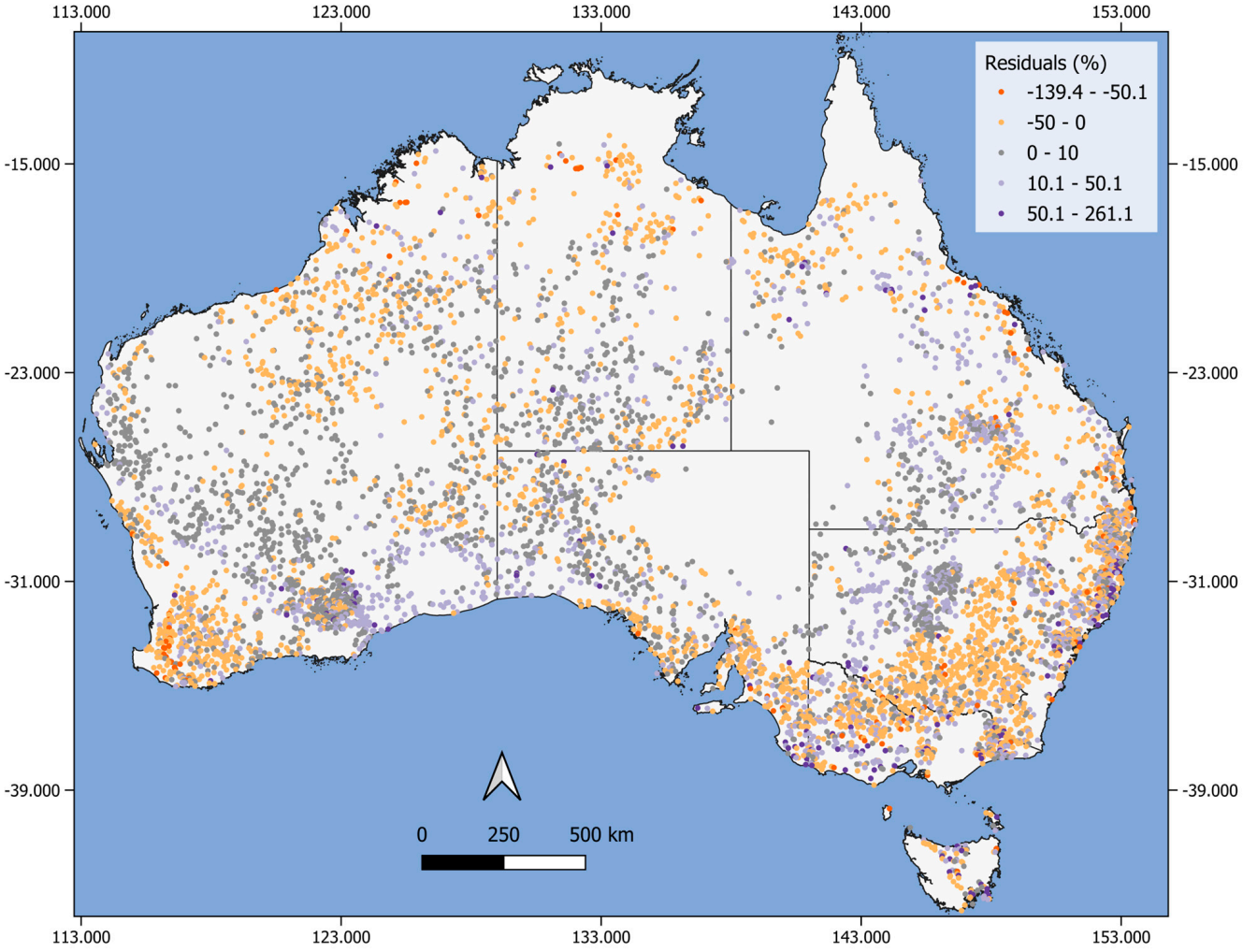


Figure 5. Spatial distribution of residuals. Residuals were calculated by subtracting the Sentinel-2 LFMC from the MODIS-based LFMC. Positive values indicate an underprediction of LFMC by the Sentinel-2 model, and negative values indicate overprediction of LFMC.

Following NDII, NDVI, and the green reflectance band are the next most important predictors in the permutation ranking. Red-edge bands also contributed at intermediate levels. The consistency between impurity-based (Gini) and permutation importance metrics supports the stability of the feature ranking and indicates that model predictions are informed by complementary spectral regions spanning the visible, red-edge, and infrared domains rather than being dominated by a single band or narrow spectral range.

3.2. Independent Quantitative Validations Using In Situ LFMC Measurements

3.2.1. Validation with Globe-LFMC 2.0

Independent quantitative validation using post-2015 Globe-LFMC 2.0 measurements in Australia revealed that model performance was strongly influenced by site homogeneity, as quantified by NDVI CV (6, Table S1). When all vegetation types were pooled, the highest agreement between Sentinel-2 predictions and in situ LFMC occurred at the most homogeneous sites ($\leq$40th percentile NDVI CV), where the model achieved $R^2 \approx 0.25$ and RMSE = 29.10% LFMC. As progressively more heterogeneous sites were included, predictive performance declined markedly, with R^2 dropping below zero for the upper NDVI CV percentiles (Figure 5).

This pattern indicates that site heterogeneity, rather than sample size, is the dominant factor limiting agreement with field observations. For example, although the number

of samples increases from 40 at the 20th percentile to 197 when using all sites, model performance deteriorates as NDVI CV rises.

Grasslands exhibited the strongest agreement between Sentinel-2 estimates and field-measured LFMC (Figures 6 and 7). In the most homogeneous sites (10th–30th NDVI_CV percentiles), model performance was high ($R^2 > 0.85$, RMSE ≈ 25%), although these thresholds included relatively few samples (<6). Performance declined gradually with increasing site heterogeneity, but remained robust even at the 60th percentile ($R^2 = 0.58$, RMSE = 34%). When all grassland samples were considered (100th percentile), the model still exhibited moderate predictive skill ($R^2 = 0.27$).

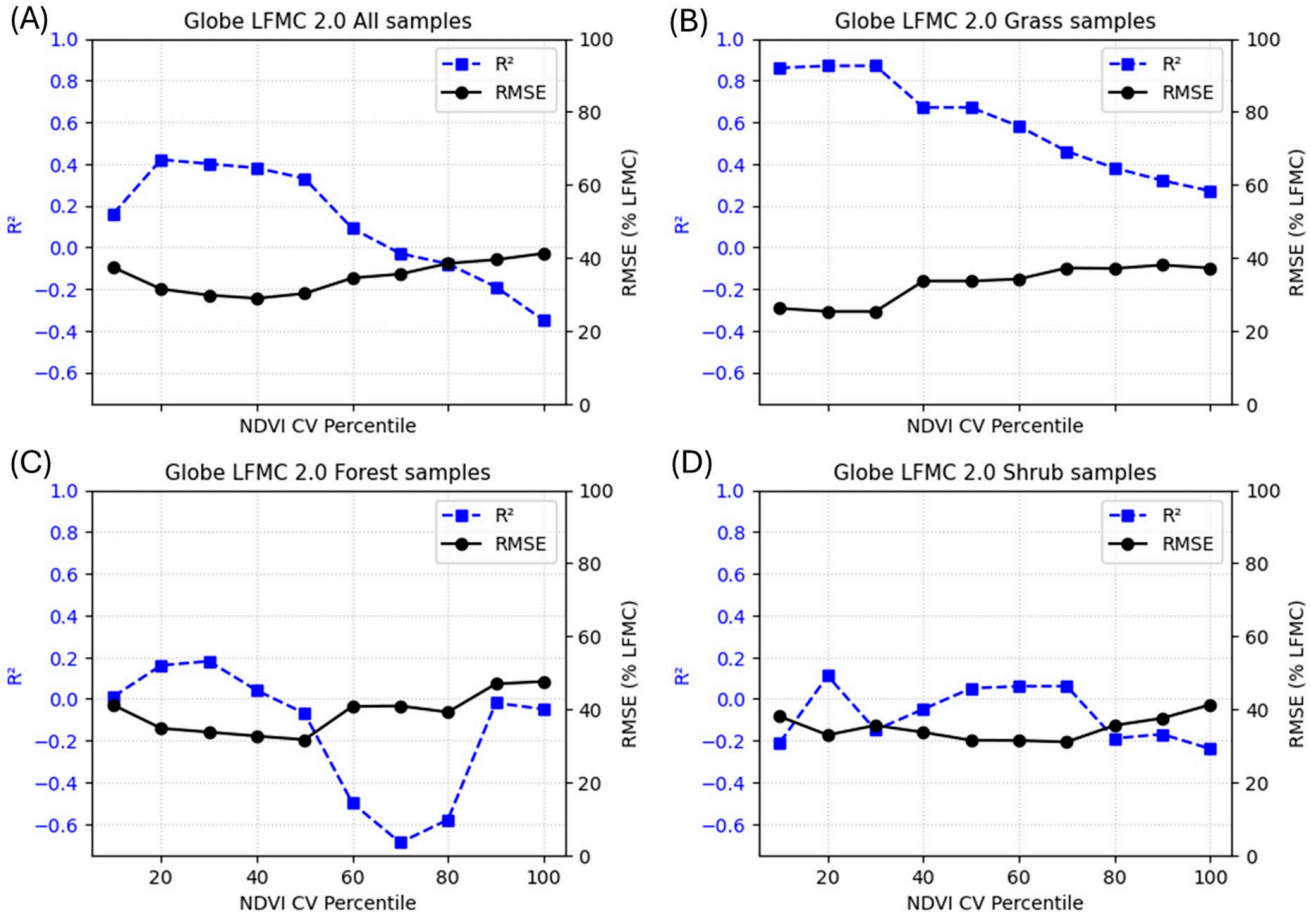


Figure 6. Effects of site homogeneity on Sentinel-2 LFMC model performance. Panel (**A**): results for all vegetation types combined; Panels (**B**–**D**): results for grasslands, forests, and shrublands, respectively. Model goodness of fit (R^2; left vertical axis, dashed line) and error (RMSE, % LFMC; right vertical axis, solid line) are shown as a function of the NDVI_CV percentile (horizontal axis). Lower NDVI_CV percentiles correspond to more homogeneous sites.

Agreement between predicted and measured LFMC in forests was modest and highly sensitive to site heterogeneity (Figures 6 and 7). The best performance was observed for the 30th NDVI_CV percentile ($R^2 = 0.18$, RMSE = 33.7%). Above this threshold, accuracy declined rapidly, and R^2 became negative for percentiles >50%, reflecting weak correspondence between field samples and surface reflectance in more heterogeneous or structurally complex sites.

Shrublands showed the weakest and most variable performance (Figure 6). For homogeneous sites (10th–30th percentiles), R^2 ranged from −0.21 to 0.11 and RMSE from 32% to 38%. Performance did not improve with additional samples at higher percentiles, indicating that heterogeneity alone does not fully explain the discrepancies.

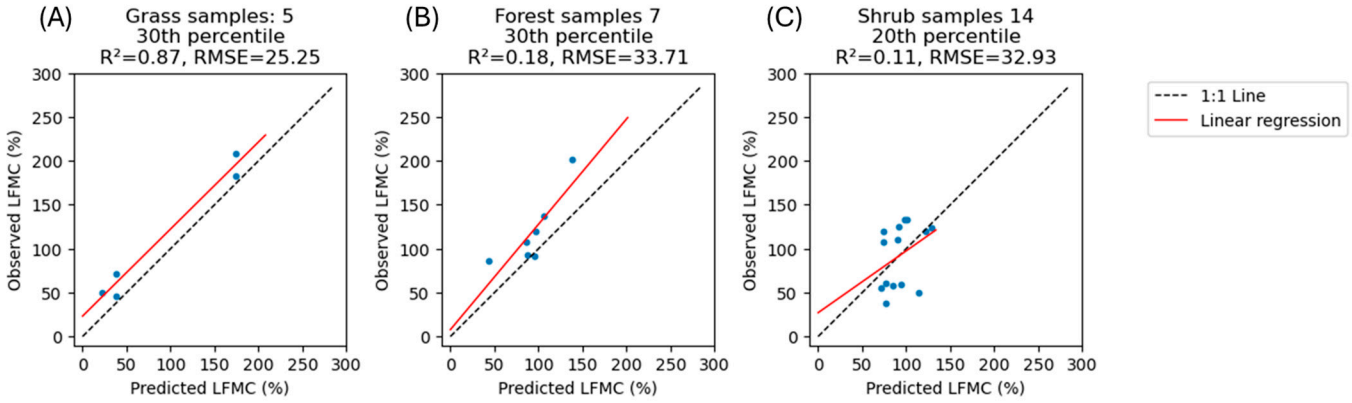


Figure 7. Validation of Sentinel-2 LFMC estimates against in situ LFMC measurements from Globe-LFMC 2.0 across three vegetation types (grasslands (**A**), forests (**B**), shrublands (**C**)), showing the site-homogeneity thresholds defined by NDVI_CV percentiles, where the correlation coefficient is highest for that vegetation type. Lower NDVI_CV percentiles correspond to more homogeneous sites.

The influence of the temporal matching window between satellite acquisition and field sampling was also evaluated (Table S2). Model performance remained broadly consistent across ±3-, ±5-, and ±10-day windows, indicating that moderate temporal offsets had limited influence on validation outcomes. Differences in R^2 and RMSE between the ±3- and ±5-day windows were generally small. Slightly improved performance was occasionally observed for the ±10-day window. However, this improvement is likely attributable to the larger number of available samples rather than to a genuine increase in predictive accuracy.

3.2.2. Dedicated Sentinel-2 LFMC Field Campaign Validation

The samples originated from a Sentinel-2 targeted validation campaign in forest environments across New South Wales and showed substantially stronger agreement with in situ LFMC than in the broader national evaluation. The mean observed LFMC for each site and date is moderately correlated with the predicted values (R^2 = 0.53), with an RMSE of 32.14% LFMC (Figure 8).

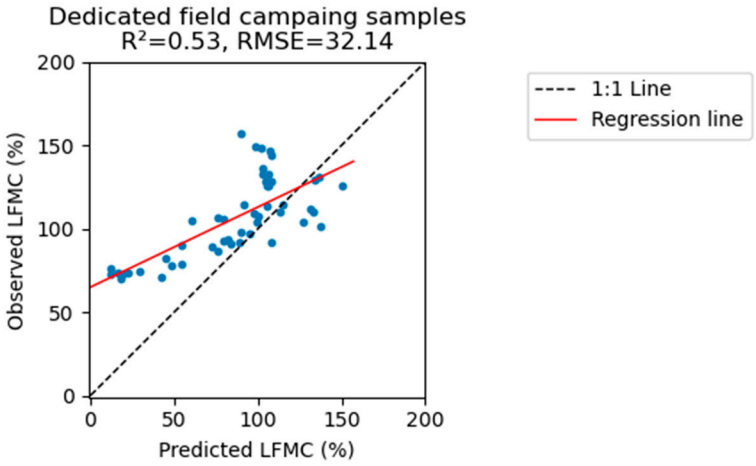


Figure 8. Comparison between observed LFMC (%) from the Sentinel-2-specific validation campaign and LFMC predicted by the Sentinel-2 emulator. All data points were used (i.e., NDVI CV = 100th percentile).

3.3. Temporal Validation Using Long-Term LFMC Time Series

Visual inspection of sites with long-term LFMC time series shows that the Sentinel-2 model successfully reproduces the seasonal dynamics observed in the in situ measurements

(Figure 9). Predicted LFMC follows the timing and magnitude of seasonal drying and recovery, with the strongest correspondence at sites with frequent monitoring, such as the Cumberland Plain SuperSite.

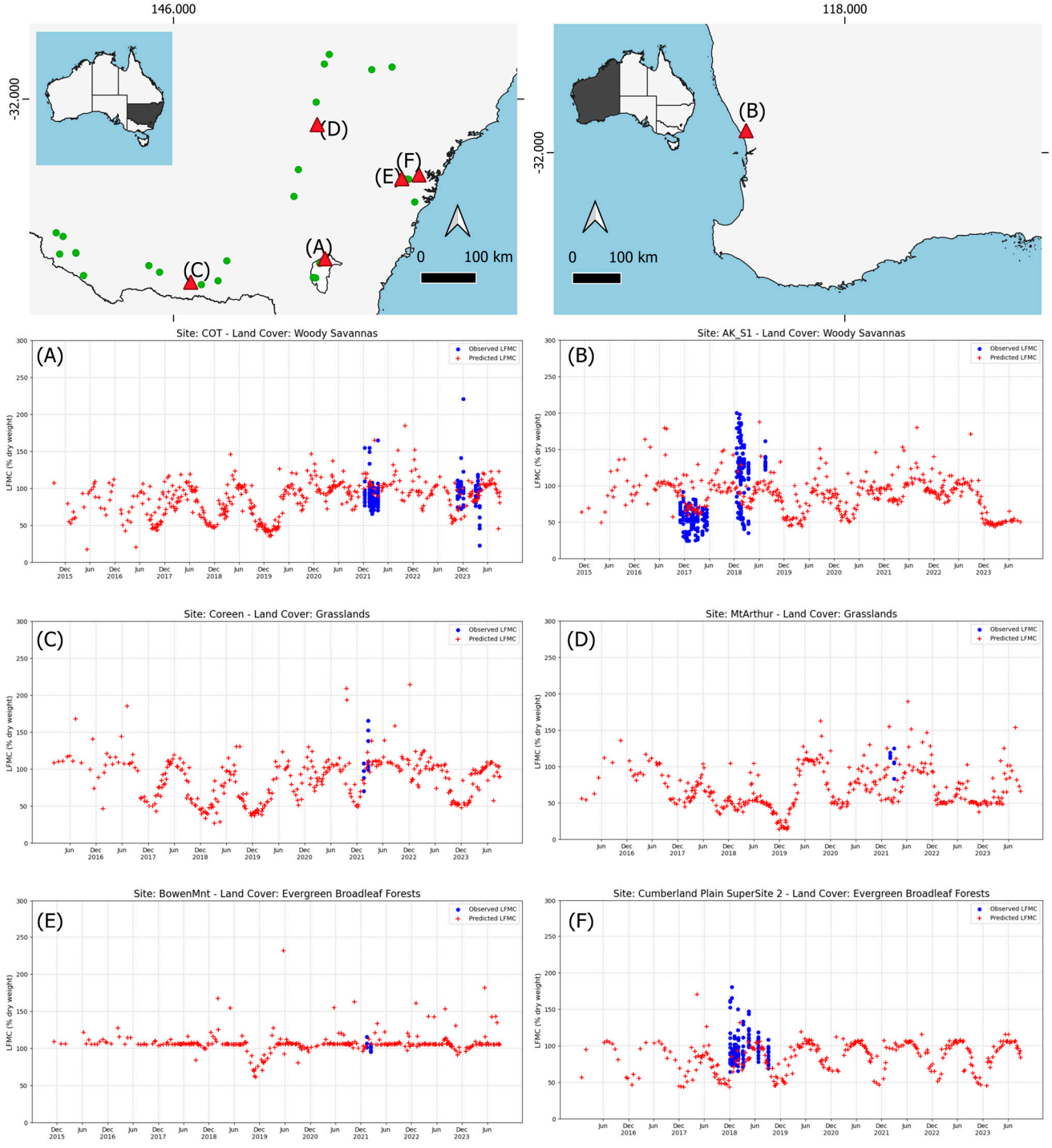


Figure 9. Comparison of predicted and observed LFMC time series for five monitoring sites across Australia. Sentinel-2 LFMC estimates are shown as red crosses (median of a 40 m × 40 m buffer around the sampling location), and in situ measurements from Globe-LFMC 2.0 as blue dots. The model effectively reproduces seasonal LFMC trends, with the strongest agreement at sites with high measurement frequency. (**A**) AK_S1 (WA, 288 samples); (**B**) AK_S2 (WA, 288 samples); (**C**) EucFACE_2 (NSW, 55 samples); (**D**) EucFACE_6 (NSW, 79 samples); (**E**) Cumberland Plain Supersite 2 (NSW, 133 samples); (**F**) Kentlyn (NSW, 23 samples). Sites with code names AK_S1 and AK_S2 were extracted from the Globe LFMC 2.0 dataset and correspond to two shrubland sampling sites located within

Yanchep National Park, approximately 30 km north of Perth, Western Australia. Land cover classification corresponds to that in the Globe LFMC 2.0 dataset, with the exception of sites AK_S1 and AK_S2, which were manually assigned to Shrublands following discussions with the collector.

3.4. Continental-Scale LFMC Dynamics

Monthly median LFMC maps for 2019 (Figure 10) reflect major climatic events, including elevated rainfall and flooding in northern Queensland early in the year, followed by widespread drying and the onset of the Black Summer fires in southeastern Australia during spring and early summer. Between January and March 2019 unusually high rainfall in northeastern Australia [30] meant that vegetation had plenty of water available for storage and growth. This increased water content is shown in the monthly median LFMC values between February and July 2019 (Figure 10 box region A). From August to December, the region showed a trend towards lower LFMC values, which coincided with the start of large-scale wildfires [30,31]. In the southeast of the country, monthly median LFMC changes were also detectable from the model (Figure 10, box region B). In this region, record low rainfall and high temperatures meant that large fuel loads were available to burn and spread fire [1,30–32]. While there are other regions where changes in LFMC occur, these examples show that the Sentinel-2 LFMC product captures the spatial and temporal dynamics of vegetation water content across Australia, providing information to decision makers across the country.

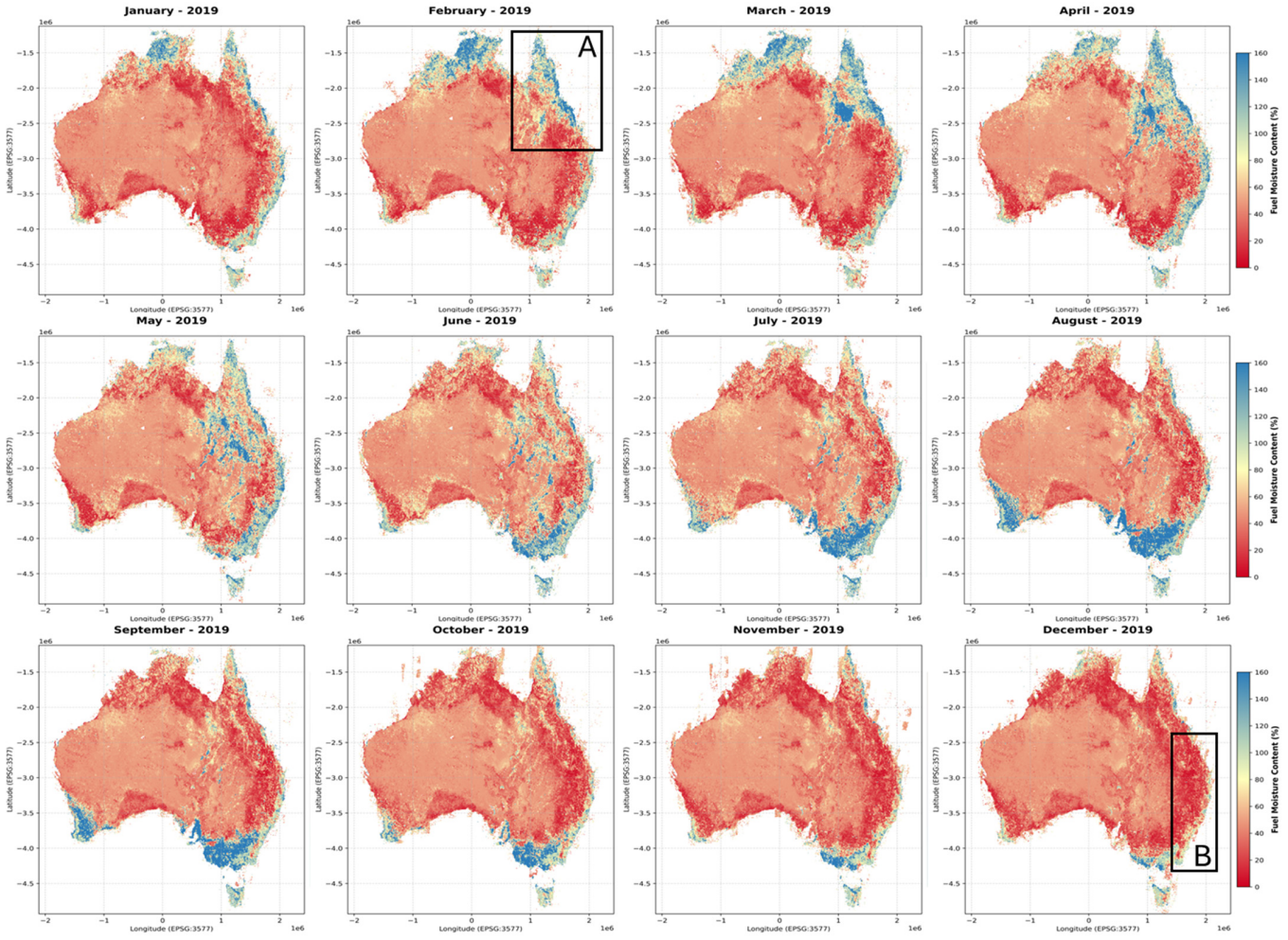


Figure 10. Monthly median LFMC estimations across Australia from January to December 2019. Colour bar range is 0–160%. Boxed regions A and B highlight northeastern and southeastern Australia,

respectively. Region A illustrates elevated LFMC following unusually high rainfall and flooding in early 2019, while Region B shows progressively lower LFMC from late winter to early summer in southeastern Australia, coinciding with record low rainfall, high temperatures, and the period preceding the 2019–2020 Black Summer fires.

4. Discussion

4.1. Emulation Accuracy (Sentinel2 LFMC Versus AFMS LFMC)

Across vegetation types, the emulator displayed systematic behaviour at the extremes of the LFMC range, tending to underestimate very high LFMC values (>250%) and overestimate extremely low values (<30%). Underestimation at the wettest end has limited operational consequence, as fuels above this threshold are unequivocally moist. Overestimation of very low LFMC is more relevant to fire danger applications; however, most inflated values remained below ~50% LFMC—already a high-risk domain [33]. A small number of outliers highlight the need for caution in site-level interpretation but do not compromise broad-scale applicability.

Emulation performance varied systematically across MODIS vegetation classes. Grasslands showed the strongest correspondence with AFMS LFMC, which reflects the wider LFMC dynamic range allowed by the MODIS-based algorithm (0–300%) and the more direct spectral–moisture relationships in herbaceous vegetation.

Shrublands exhibited the weakest emulation accuracy, consistent with structural constraints inherited from the AFMS shrubland algorithm. The radiative-transfer inversion used for AFMS shrublands restricts LFMC to ~50–130% [5], preventing the model from expressing the full physiological range. This limited variability propagates into the emulator's training set, weakening its ability to learn robust LFMC–reflectance relationships. Unlike the MODIS algorithm, the Sentinel-2 emulator does not enforce LUT-based physical constraints and can generate LFMC > 200% when shrubland reflectance resembles that of grasslands or mixed pixels, an artefact of limited training variability rather than sensor behaviour.

Forests showed intermediate performance with agreement being the strongest within the central, data-rich portion of the LFMC range, with larger errors at the low and high extremes where training samples were sparse. Forest spectral complexity, combining tree crowns, shadows, stems, and understorey vegetation, reduces the distinctiveness of LFMC signals relative to grasslands. In addition, the narrower AFMS forest LUT range provides less functional contrast for the emulator to learn from. Together, these factors limit emulation precision in forests despite Sentinel-2's high spatial resolution.

4.2. Independent Validation Using In Situ LFMC Measurements

Independent validation using Globe-LFMC 2.0 confirmed that agreement between predicted and measured LFMC depends strongly on site homogeneity and sampling representativeness. The highest R^2 values were generally observed at the most homogeneous sites (lowest NDVI_CV), particularly in grasslands and forests. As spatial heterogeneity increased, predictive power declined. This demonstrates that part of the model–measurement discrepancy originates from mismatches between what the satellite observes (a 40 m $\times$ 40 m mixed region) and what field protocols typically measure (a single vegetation stratum). Temporal offsets of up to $\pm$10 days between field sampling and the nearest available Sentinel-2 acquisition were also evaluated, but differences in model performance across temporal matching windows were small.

The mismatch between satellite pixel composition and field sampling protocols is most apparent in open-canopy forests and shrublands, where Sentinel-2 reflectance captures a mixture of tree crowns, grasses, shrubs, and soil. Many Globe-LFMC 2.0 measurements capture only one of these components, most commonly tree foliage, thereby under-representing

the vegetation mixture observed by the satellite. As progressively more heterogeneous sites were included in validation, RMSE increased, and R^2 decreased, consistent with mixed-pixel effects rather than emulator failure.

Shrublands again showed the lowest validation performance, reflecting both inherited LUT constraints and additional limitations in the in situ dataset. Globe-LFMC 2.0 shrubland samples were collected using two distinct protocols: fresh-weight measurements in the field versus fresh-weight measurements in the laboratory. These methodological differences systematically affect the calculated LFMC, producing two artificial clusters of values unrelated to vegetation differences. This protocol-induced variance reduces the apparent predictive accuracy of the Sentinel-2 emulator in shrublands.

Model performance improved substantially when evaluated against samples from a dedicated field campaign explicitly designed for Sentinel-2 LFMC validation. Under unified sampling protocols, matched spatial footprints, and closely aligned sampling dates, the emulator achieved markedly higher accuracy, outperforming results obtained using the broader and more heterogeneous dataset for forested sites. These findings confirm that when field measurements accurately represent the Sentinel-2 pixel, the emulator can reproduce LFMC with considerably greater fidelity, and emphasise the critical role of sampling design in remote-sensing validation.

When contextualised against other Sentinel-2 LFMC studies conducted at site or regional scales, our validation results fall within the performance envelope commonly reported in the literature. Under geographically constrained domains, locally calibrated and structurally homogeneous conditions, R^2 values typically vary between ~0.4–0.7 and RMSE between 8–25% LFMC. These performances are similar or slightly better than results from multi-sensor approaches at landscape scales (e.g., SAR-optical (Landsat or Sentinel-2) models with $R^2 \approx 0.3$–0.7, RMSE $\approx$ 25–31%) [34,35].

Direct numerical comparison across studies remains challenging due to differences in vegetation types, spatial resolution, calibration strategies, validation protocols, and LFMC dynamic ranges. Nevertheless, a consistent finding across the literature is that performance is strongly influenced by site homogeneity, representativeness of the training data, and the scale at which models are developed and validated.

In contrast, the present study evaluates a continental-scale operational product across diverse ecosystems, heterogeneous vegetation structures, and mixed sampling protocols, without local recalibration. Therefore, the comparatively lower R^2 values observed in parts of the national-scale validation primarily reflect differences in representativeness, structural complexity, and spatial scale, rather than intrinsic limitations of Sentinel-2 reflectance for LFMC estimation

The emulator also successfully captured temporal LFMC dynamics, reproducing seasonal drying and recovery patterns observed in Globe-LFMC 2.0 time series. This behaviour is particularly valuable for identifying seasonal windows for prescribed burning, monitoring post-treatment fuel recovery, and assessing shifts in vegetation moisture under climate extremes. Temporal alignment between predicted and measured LFMC demonstrates that, even where absolute accuracy varies among vegetation types, the emulator captures the ecologically meaningful temporal trajectories required for many fire-management applications.

4.3. Implications and Limitations

Three interacting factors underpin the observed discrepancies between the Sentinel-2 LFMC product, the MODIS-based AFMS estimates, and independent field measurements: (i) limitations inherited from the AFMS model, including restricted LFMC ranges for forests and shrublands; (ii) structural mismatches between satellite footprints and field

sampling protocols; and (iii) the inherent constraints of statistical emulation. Because the emulator approximates a model that itself contains structural uncertainty, deviations from field measurements reflect combined effects of the AFMS model, the emulator, and representativeness limitations in the in situ dataset. Insufficient field data represents another challenge for the validation of the product. When data are aggregated by site and date, low sample sizes lead to undetermined performance in some vegetation types (e.g., savannas, Supplementary Materials); in these cases, additional field data covering large spatial extents are needed to accurately assess the performance of the model.

These limitations are particularly evident in shrubland ecosystems, where the spatial coverage of validation samples was most limited; LFMC estimations should be interpreted with caution. In these ecosystems, the Sentinel-2 LFMC product is more appropriately used to monitor relative spatial (Figure 3) and temporal (e.g., Figures 9 and 10) variability, as opposed to inferring absolute moisture values. The ability of this product to capture the LFMC dynamics over space and time supports the identification of seasonal drying patterns and anomalous moisture conditions, thereby contributing to improved understanding of vegetation responses to long-term climatic variability and change. Despite these constraints, the emulator demonstrates strong capacity to reproduce AFMS variability, reasonable accuracy against independent field measurements under representative conditions, and robust temporal dynamics (Figure 10, Table 2). These properties make the Sentinel-2 LFMC product suitable for proactive fuel management interventions, conservation and land management planning, and a range of operational and strategic fire management applications, including landscape-scale fuel monitoring, prescribed burn planning, and integration into fire behaviour and air quality and emissions modelling frameworks.

Table 2. Summary of Advantages, limitations, and operational applications of the Sentinel-2 LFMC data product.

Category	Description
Advantages	High spatial resolution (20 m) with frequent (5-day) updates across Australia.
	Computationally efficient implementation.
	Spatial detail enables differentiation of fine-scale heterogeneity (e.g., fuel discontinuities, roads, management boundaries).
	Operational continuity with the AFMS framework, ensuring consistency with existing fuel monitoring practices.
	Historical archive available from 2015, enabling multi-year analysis and anomaly detection.
	Near-real-time operational product suitable for integration into wildfire information systems
	Open-source and reproducible workflow that can be adapted to other regions.
Limitations	LFMC range partly inherited from the AFMS training domain, limiting representation of extreme values.
	Performance sensitive to site heterogeneity and representativeness of in situ validation data
	Structural uncertainty due to emulation of a MODIS-based product rather than direct physical LFMC retrieval.
	Currently calibrated for three broad vegetation classes (grasslands, shrublands, forests)

Table 2. *Cont.*

Category	Description
Operational Applications	Landscape-scale monitoring of vegetation dryness and seasonal fuel condition dynamics
	Support for prescribed burn planning and fuel treatment assessment (e.g., identifying periods and locations where fuels approach operational ignition thresholds).
	Input to fire behaviour, emissions, and air-quality models
	Risk modelling applications across environmental, infrastructure, health, and financial domains, where seasonal exceedance of critical ignition thresholds can inform probabilistic loss and exposure models

4.4. Future Directions

Several avenues have been identified to further improve this novel dataset. A primary priority is the inclusion of a per-pixel uncertainty flag to inform users about the reliability of LFMC estimates. Such uncertainty later would not imply a direct dependence of the Sentinel-2 LFMC model on a specific land cover product, but would instead characterise structural sources of uncertainty associated with each pixel. These may include the spatial resolution and classification accuracy of the IGBP land cover and MODIS datasets (e.g., Figure 3), the representativeness and spatial distribution of ground validation samples, and the temporal stability of the land cover classes. In particular, pixels located in heterogeneous or transitional landscapes, in vegetation types with limited validation coverage, or in ecosystems such as shrublands where model performance was comparatively lower, may exhibit inherently higher uncertainty.

Another key improvement involves the integration of more recent and spatially detailed land cover products. This would help reduce mixed-pixel effects and improve vegetation class assignment, particularly in heterogeneous landscapes where coarse land cover maps may introduce structural uncertainty.

In the longer term, advances in computational resources and machine learning methodologies may enable direct estimation of LFMC from Sentinel-2 reflectance and ancillary data, bypassing the limitations inherited from the MODIS-based model. At the same time, coordinated and standardised field sampling efforts targeting underrepresented regions and vegetation types in current databases, such as Globe-LFMC [17] will be critical to improving model generalisability and reducing structural uncertainty. Future efforts should therefore prioritise expanded in situ calibration/validation campaigns across diverse ecosystems, using standardised protocols that explicitly capture both canopy and understorey components. Such measurements are essential to better characterise what the satellite sensor effectively integrates within its footprint, particularly across fuel types with varying vertical structural complexity.

5. Conclusions

We present a national Sentinel-2 LFMC product designed to support both strategic and operational fire management activities in Australia. By emulating the MODIS-based LFMC model currently used within the Australian Flammability Monitoring System, the Sentinel-2 approach provides a more spatially detailed and computationally efficient alternative while maintaining broad consistency with AFMS-derived LFMC patterns. Emulation performance varied across vegetation types, with the strongest agreement in grasslands and lower fidelity in shrublands and open forests due to inherited AFMS constraints and representativeness limitations in available in situ datasets.

Validation against Globe-LFMC 2.0 showed modest but encouraging accuracy, especially at spatially homogeneous sites where field measurements more closely reflect

the Sentinel-2 footprint. Temporal mismatch between field measurements and satellite observations was not the primary source of validation of uncertainty. Purpose-designed field campaigns aligned with the Sentinel-2 spatial and temporal sampling strategy yielded substantially higher accuracy, demonstrating that the emulator performs best when validated with representative, harmonised in situ measurements. The model also captured seasonal LFMC dynamics at long-term monitoring sites, highlighting its potential utility for seasonal fuel moisture monitoring and prescribed-burn planning.

Given its high spatial and temporal resolution, the Sentinel-2 LFMC dataset provides valuable information for a wide range of applications, including delineating ignitable zones for prescribed burns, monitoring fuel treatments (e.g., mechanical thinning, hazard reduction burns), characterising landscape-scale fuel dynamics, and informing fire behaviour and emission or air-quality models. Beyond fire agencies, this dataset offers actionable intelligence for sectors such as insurance, infrastructure planning, health, and community risk reduction. Importantly, the product also offers opportunities for Indigenous and First Nations land managers to combine satellite-derived fuel moisture information with cultural knowledge systems to support cultural burning and land stewardship (see e.g., https://youtu.be/tLgqBDuSOdU?si=oDJWn4Wz71M0qNLf, accessed on 20 March 2025).

Despite limitations in specific vegetation types, the Sentinel-2 LFMC product represents a significant advancement in operational fuel moisture monitoring and provides a foundation for continued refinement through improved validation datasets, updated land-cover information, and next-generation modelling approaches.

Supplementary Materials: The following supporting information can be downloaded at: https://www.mdpi.com/article/10.3390/rs18071049/s1.

Author Contributions: Conceptualization: M.Y. and A.I.J.M.v.D.; Data curation: G.S. and N.Y.; Formal analysis: G.S. and N.Y.; Funding acquisition: M.Y.; Investigation: M.Y., G.S. and N.Y.; Methodology: M.Y., G.S. and A.I.J.M.v.D.; Project administration: M.Y.; Supervision: M.Y.; Validation: G.S. and N.Y.; Visualisation: G.S. and N.Y.; Writing—original draft preparation: G.S. and M.Y.; Writing—review and editing: all authors. All authors have read and agreed to the published version of the manuscript.

Funding: Funding for this project was provided by the Natural Hazards Research Australia (NHRA).

Data Availability Statement: Sentinel-2 data are freely available through the European Space Agency Copernicus Programme and through Geoscience Australia's Digital Earth Australia. The Sentinel-2 Fuel Moisture Content product is freely available through Digital Earth Australia (https://doi.org/10.26186/150554). The data presented in this study are available through the Globe LFMC 2.0 dataset [17] and through the official GitHub repository for this project (https://github.com/BRCoE/sentinel2_FMC_emulator_v2, accessed on 20 March 2025).

Acknowledgments: We would like to thank Pablo Larraondo for developing the prototype framework for extracting the input data cube (https://github.com/BRCoE/sentinel2_FMC_emulator_v2, accessed on 20 March 2025) and the Bushfire Research Centre of Excellence (ANU) for in-kind support). During the preparation of this work, the authors used ChatGPT (v4) to improve readability and the language of the manuscript. After using this tool/service, the authors reviewed and edited the content as needed and takes full responsibility for the content of the published article.

Conflicts of Interest: The authors declare no conflict of interest.

References

1. Cunningham, C.X.; Williamson, G.J.; Bowman, D.M.J.S. Increasing Frequency and Intensity of the Most Extreme Wildfires on Earth. *Nat. Ecol. Evol.* **2024**, *8*, 1420–1425. [CrossRef] [PubMed]
2. State of Wildfires Project. State of Wildfires 2024–2025: Summary for Policymakers. State of Wildfires Project. 2025. Available online: https://stateofwildfires.com/latest-report/ (accessed on 20 March 2025).

3. Yebra, M.; Dennison, P.E.; Chuvieco, E.; Riaño, D.; Zylstra, P.; Hunt, E.R.; Danson, F.M.; Qi, Y.; Jurdao, S. A Global Review of Remote Sensing of Live Fuel Moisture Content for Fire Danger Assessment: Moving towards Operational Products. *Remote Sens. Environ.* **2013**, *136*, 455–468. [CrossRef]
4. Chuvieco, E.; Yebra, M.; Martino, S.; Thonicke, K.; Gómez-Giménez, M.; San-Miguel, J.; Oom, D.; Velea, R.; Mouillot, F.; Molina, J.R.; et al. Towards an Integrated Approach to Wildfire Risk Assessment: When, Where, What and How May the Landscapes Burn. *Fire* **2023**, *6*, 215. [CrossRef]
5. Yebra, M.; Quan, X.; Riaño, D.; Rozas Larraondo, P.; van Dijk, A.I.J.M.; Cary, G.J. A Fuel Moisture Content and Flammability Monitoring Methodology for Continental Australia Based on Optical Remote Sensing. *Remote Sens. Environ.* **2018**, *212*, 260–272. [CrossRef]
6. Chuvieco, E.; Aguado, I.; Salas, J.; García, M.; Yebra, M.; Oliva, P. Satellite Remote Sensing Contributions to Wildland Fire Science and Management. *Curr. For. Rep.* **2020**, *6*, 81–96. [CrossRef]
7. Cunill Camprubí, À.; González-Moreno, P.; Resco de Dios, V. Live Fuel Moisture Content Mapping in the Mediterranean Basin Using Random Forests and Combining MODIS Spectral and Thermal Data. *Remote Sens.* **2022**, *14*, 3162. [CrossRef]
8. Jurdao, S.; Yebra, M.; Guerschman, J.P.; Chuvieco, E. Regional Estimation of Woodland Moisture Content by Inverting Radiative Transfer Models. *Remote Sens. Environ.* **2013**, *132*, 59–70. [CrossRef]
9. Nolan, R.H.; Boer, M.M.; Resco de Dios, V.; Caccamo, G.; Bradstock, R.A. Large-Scale, Dynamic Transformations in Fuel Moisture Drive Wildfire Activity across Southeastern Australia. *Geophys. Res. Lett.* **2016**, *43*, 4229–4238. [CrossRef]
10. Quan, X.; Chen, R.; Yebra, M.; Riaño, D.; Resco de Dios, V.; Li, X.; He, B.; Nolan, R.H.; Griebel, A.; Boer, M.M.; et al. Sub-Daily Live Fuel Moisture Content Estimation from Himawari-8 Data. *Remote Sens. Environ.* **2024**, *308*, 114170. [CrossRef]
11. Drusch, M.; Del Bello, U.; Carlier, S.; Colin, O.; Fernandez, V.; Gascon, F.; Hoersch, B.; Isola, C.; Laberinti, P.; Martimort, P.; et al. Sentinel-2: ESA's Optical High-Resolution Mission for GMES Operational Services. *Remote Sens. Environ.* **2012**, *120*, 25–36. [CrossRef]
12. Marino, E.; Yebra, M.; Guillén-Climent, M.; Algeet, N.; Tomé, J.L.; Madrigal, J.; Guijarro, M.; Hernando, C. Investigating Live Fuel Moisture Content Estimation in Fire-Prone Shrubland from Remote Sensing Using Empirical Modelling and RTM Simulations. *Remote Sens.* **2020**, *12*, 2251. [CrossRef]
13. Marino, E.; Yáñez, L.; Guijarro, M.; Madrigal, J.; Senra, F.; Rodríguez, S.; Tomé, J.L. Transferability of Empirical Models Derived from Satellite Imagery for Live Fuel Moisture Content Estimation and Fire Risk Prediction. *Fire* **2024**, *7*, 276. [CrossRef]
14. Chotamonsak, C.; Lapyai, D.; Thanadolmethaphorn, P. Towards Near-Real-Time Estimation of Live Fuel Moisture Content from Sentinel-2 for Fire Management in Northern Thailand. *Fire* **2025**, *8*, 475. [CrossRef]
15. Costa-Saura, J.M.; Balaguer-Beser, Á.; Ruiz, L.A.; Pardo-Pascual, J.E.; Soriano-Sancho, J.L. Empirical Models for Spatio-Temporal Live Fuel Moisture Content Estimation in Mixed Mediterranean Vegetation Areas Using Sentinel-2 Indices and Meteorological Data. *Remote Sens.* **2021**, *13*, 3726. [CrossRef]
16. Tanase, M.A.; Nova, J.P.; Marino, E.; Aponte, C.; Tomé, J.L.; Yáñez, L.; Madrigal, J.; Guijarro, M.; Hernando, C. Characterizing Live Fuel Moisture Content from Active and Passive Sensors in a Mediterranean Environment. *Forests* **2022**, *13*, 1846. [CrossRef]
17. Yebra, M.; Scortechini, G.; Adeline, K.; Aktepe, N.; Almoustafa, T.; Bar-Massada, A.; Beget, M.E.; Boer, M.; Bradstock, R.; Brown, T.; et al. Globe-LFMC 2.0, an Enhanced and Updated Dataset for Live Fuel Moisture Content Research. *Sci. Data* **2024**, *11*, 332. [CrossRef]
18. GA. *DEA Fuel Moisture Content (Sentinel-2)*; GA: Canberra, Australia, 2025.
19. Pedregosa, F.; Varoquaux, G.; Gramfort, A.; Michel, V.; Thirion, B.; Grisel, O.; Blondel, M.; Prettenhofer, P.; Weiss, R.; Dubourg, V.; et al. Scikit-Learn: Machine Learning in Python. *J. Mach. Learn. Res.* **2011**, *12*, 2825–2830.
20. Schaaf, C.; Wang, Z. MODIS/Terra + Aqua BRDF/Albedo Nadir BRDF Adjusted Ref Daily L3 Global—500m V061 [Data set]. Land Processes Distributed Active Archive Center. 2021. Available online: https://www.earthdata.nasa.gov/data/catalog/lpcloud-mcd43a4-061 (accessed on 20 March 2025).
21. Geoscience Australia. *Sentinel-2A MSI NBART Collection 3—DEA Surface Reflectance NBART (Sentinel-2A MSI)*; Geoscience Australia: Canberra, Australia, 2022.
22. Li, F.; Jupp, D.L.B.; Thankappan, M.; Lymburner, L.; Mueller, N.; Lewis, A.; Held, A. A Physics-Based Atmospheric and BRDF Correction for Landsat Data over Mountainous Terrain. *Remote Sens. Environ.* **2012**, *124*, 756–770. [CrossRef]
23. Tucker, C.J.; Sellers, P.J. Satellite Remote Sensing of Primary Production. *Int. J. Remote Sens.* **1986**, *7*, 1395–1416. [CrossRef]
24. Yilmaz, M.T.; Hunt, E.R.; Jackson, T.J. Remote Sensing of Vegetation Water Content from Equivalent Water Thickness Using Satellite Imagery. *Earth Obs. Terr. Biodivers. Ecosyst. Spec. Issue* **2008**, *112*, 2514–2522. [CrossRef]
25. ODC Open Data Cube. Available online: https://opendatacube.readthedocs.io/en/latest/api/indexed-data/generate/datacube.Datacube.load.html (accessed on 20 March 2025).
26. Kotzur, I.; Boer, M.; Yebra, M.; Moore, B.D. Monitoring Forest Foliar Moisture Using Sentinel-2 Reflectance and Radiative Transfer Model Inversion. *bioRxiv* **2025**. bioRxiv:2025.06.25.661444. [CrossRef]

27. Jamieson, K.; Talwalkar, A. Non-Stochastic Best Arm Identification and Hyperparameter Optimization. In *Proceedings of the Proceedings of the 19th International Conference on Artificial Intelligence and Statistics*; Gretton, A., Robert, C.C., Eds.; PMLR: Brookline, MA, USA, 2016; Volume 51, pp. 240–248.
28. Quan, X.; Yebra, M.; Riaño, D.; He, B.; Lai, G.; Liu, X. Global Fuel Moisture Content Mapping from MODIS. *Int. J. Appl. Earth Obs. Geoinf.* **2021**, *101*, 102354. [CrossRef]
29. Friedl, M.; Sulla-Menashe, D. *MODIS/Terra + Aqua Land Cover Type Yearly L3 Global 500m SIN Grid V061 [Data Set]*; NASA Land Processes Distributed Active Archive Center: Sioux Falls, SD, USA, 2022.
30. Australian Institute for Disaster Resilience. *AIDR Major Incidents Report 2018–2019*; Australian Institute for Disaster Resilience: East Melbourne, Australia, 2019.
31. Australian Institute for Disaster Resilience. *AIDR Major Incidents Report 2019–2020*; Australian Institute for Disaster Resilience: East Melbourne, Australia, 2020.
32. Nolan, R.H.; Bowman, D.M.J.S.; Clarke, H.; Haynes, K.; Ooi, M.K.J.; Price, O.F.; Williamson, G.J.; Whittaker, J.; Bedward, M.; Boer, M.M.; et al. What Do the Australian Black Summer Fires Signify for the Global Fire Crisis? *Fire* **2021**, *4*, 97. [CrossRef]
33. Argañaraz, J.P.; Landi, M.A.; Scavuzzo, C.M.; Bellis, L.M. Determining Fuel Moisture Thresholds to Assess Wildfire Hazard: A Contribution to an Operational Early Warning System. *PLoS ONE* **2018**, *13*, e0204889. [CrossRef]
34. Rao, K.; Williams, A.P.; Flefil, J.F.; Konings, A.G. SAR-Enhanced Mapping of Live Fuel Moisture Content. *Remote Sens. Environ.* **2020**, *245*, 111797. [CrossRef]
35. Wang, C.; Zhang, B.; Zhu, L.; Yang, K.; Lu, B.; Su, B.; Chen, Z. Estimation of Live Fuel Moisture Content via Spectral–Meteorological Time-Series Fusion: A TCN–BiGRU Deep Learning Framework. *Int. J. Remote Sens.* **2026**, 1–33. [CrossRef]

Disclaimer/Publisher's Note: The statements, opinions and data contained in all publications are solely those of the individual author(s) and contributor(s) and not of MDPI and/or the editor(s). MDPI and/or the editor(s) disclaim responsibility for any injury to people or property resulting from any ideas, methods, instructions or products referred to in the content.